Sterically Controlled Architectural Reversion in Hydrogen-Bonded Crystalline Clathrates

Cara C. Evans, Lisa Sukarto, and Michael D. Ward*

Contribution from the Department of Chemical Engineering and Materials Science, University of Minnesota, 421 Washington Ave. S.E., Minneapolis, Minnesota 55455

Received August 31, 1998

Abstract: Guanidinium cations and azobenzene-4,4′-disulfonate (**ABDS**) dianions form a host lattice with a bilayer architecture in the presence of 1,4-dibromobenzene (DBB), 1,4-divinylbenzene (DVB), 1-nitronaphthalene (NN), and nitrobenzene (NB) guest molecules. The guests occupy one-dimensional pores in bilayer galleries created by **ABDS** dianions, which behave as "pillars" that connect opposing hydrogen-bonded guanidinium-sulfonate (**GS**) sheets. This contrasts with our previous observation of a high porosity "brick" framework that crystallized with these guests when the pillar was biphenyl-4,4′-disulfonate (**BPDS**). The reversion to the bilayer framework upon changing to **ABDS** can be attributed to the increased length of this pillar. Whereas the four guests are too large to fit in the pores of an ideal bilayer framework constructed from **BPDS**, they can be accommodated in bilayer galleries of increased height provided by the longer **ABDS** pillars. The control of framework architecture in this manner demonstrates that the solid-state structure of these materials can be rationally manipulated by systematic, stepwise adjustments to the size of the host components and of the guests. The ability to tune the pore volume of these frameworks so that different guests can be included, while retaining the essential structural features of the **GS** hosts, provides a versatile route to the synthesis of functional clathrates.

Introduction

Prediction of the solid-state structure of molecular crystals is commonly frustrated by the complexity and lack of directionality of intermolecular forces.[1] This is particularly true of porous molecular frameworks and related clathrates[2,3] which, in the absence of suitable guest molecules occupying framework voids, tend to collapse to more dense structures. Nevertheless, efforts aimed toward the synthesis of new clathrates are expanding, largely due to the potential applications for catalysis, optoelectronics, magnetics, and chemical separations.

The assembly of clathrate host frameworks frequently relies on noncovalent recognition of topologically and chemically complimentary functional groups on the molecular components. For example, open networks have been constructed using strategies based on coordination of polyvalent ligands to metal centers[3c−e,4] or intermolecular hydrogen bonding.[3f−k,5] Despite these efforts, systematic control of solid-state architecture remains difficult, owing to facile polymorphism[6] and the structural sensitivity of clathrate frameworks to even minor changes in the molecular components.[3a,7]

We recently demonstrated that control of three-dimensional (3-D) solid-state structure in molecular crystals can be simplified by the use of structurally persistent two-dimensional (2-D) networks that serve as supramolecular building blocks.[8] Specifically, numerous crystalline materials with lamellar solid-state architectures were generated from hydrogen-bonded sheets consisting of topologically and chemically complementary guanidinium (G) cations and a variety of organomonosulfonate (**S**) anions (Scheme 1). The organic residues of the **S** ions projected from the surface of the **GS** sheet, thereby introducing functionality to these layered materials. The **GS** sheets exhibited an unprecedented resilience because of their ability to adjust to the steric demands of different organic residues by (i) accordian-like puckering, defined by the angle θ_{IR}, about an axis traversing hydrogen bonds that connect one-dimensional (1-D) **GS** "ribbons," (ii) formation of "quasihexagonal" or "shifted-ribbon" hydrogen-bonding motifs, and (iii) stacking either as bilayers for small organic residues or, for larger residues, as continuously

* To whom correspondence should be addressed. Phone: (612) 625-3062. FAX: (612) 626-7246. E-mail: wardx004@tc.umn.edu.

(1) Gavezzotti, A. *Acc. Chem. Res.* **1994**, *27*, 309−314.

(2) Bishop, R. *Chem. Soc. Rev.* **1996**, 311−319.

(3) (a) Fujita, M.; Kwon, Y. J.; Sasaki, O.; Yamaguchi, K.; Ogura, K. *J. Am. Chem. Soc.* **1995**, *117*, 7287−7288. (b) Ermer, O. *J. Am. Chem. Soc.* **1988**, *110*, 3747−3754. (c) Venkataraman, D.; Lee, S.; Zhang, J.; Moore, J. S. *Nature* **1994**, *371*, 591−593. (d) Melendez, R. E.; Sharma, C. V. K.; Zaworotko, M. J.; Bauer, C.; Rogers, R. D. *Angew. Chem., Int. Ed. Engl.* **1996**, *35*, 2213−2215. (e) Yaghi, O. M.; Davis, C. E.; Li, G.; Li, H. *J. Am. Chem. Soc.* **1997**, *119*, 2861−2868. (f) Brunet, P.; Simard, M.; Wuest, J. D. *J. Am. Chem. Soc.* **1997**, *119*, 2737−2738. (g) Kolotuchin, S. V.; Fenton, E. E.; Wilson, S. R.; Loweth, C. J.; Zimmerman, S. C. *Angew. Chem., Int. Ed. Engl.* **1996**, *34*, 4, 2654−2657. (h) Aoyama, Y.; Endo, Y.; Anzai, T.; Yamaguchi, Y.; Tomoya, S.; Kobayashi, K.; Kanehisa, N.; Hashimoto, H.; Kai, Y.; Masuda, H. *J. Am. Chem. Soc.* **1996**, *118*, 5562−5571. (i) Hollingsworth, M. D.; Brown, M. E.; Hillier, A. C.; Santasiero, B. D.; Chaney, J. D. *Science* **1996**, *273*, 1355−1359. (j) Ramamurthy, V.; Eaton, D. *Chem. Mater.* **1994**, *6*, 1128−1136. (k) Herbstein, F. H. *Compr. Supramol. Chem.* **1996**, *6*, 61−83.

(4) Aäkeroy, C. B.; Nieuwenhuyzen, M. *J. Mol. Struct.* **1996**, *374*, 223−239.

(5) Ermer, O.; Lindenberg, L. *Helv. Chim. Acta* **1991**, *74*, 825−877.

(6) Ung, A. T.; Bishop, R.; Craig, D. C.; Dance, I. G.; Scudder, M. L. *Tetrahedron Lett.* **1993**, *49*, 639−648.

(7) (a) Sada, K.; Kondo, T.; Yasuda, Y.; Miyata, M.; Miki, K. *Chem. Lett.* **1994**, 727−730. (b) Hennigar, T. L.; MacQuarrie, D. C.; Losier, P.; Rogers, R. D.; Zaworotko, M. J. *Angew. Chem., Int. Ed. Engl.* **1997**, *36*, 972−973.

(8) (a) Russell, V. A.; Ward, M. D. *Chem. Mater.* **1996**, *8*, 1654−1666. (b) Russell, V. A.; Etter, M. C.; Ward, M. D. *J. Am. Chem. Soc.* **1994**, *116*, 1941−1952. (c) Russell, V. A.; Etter, M. C.; Ward, M. D. *Chem. Mater.* **1994**, *6*, 1206−1217. (d) Russell, V. A.; Ward, M. D. *J. Mater. Chem.* **1997**, *7*, 1123−1133.

10.1021/ja983122o CCC: $18.00
Published on Web 12/29/1998

Scheme 1

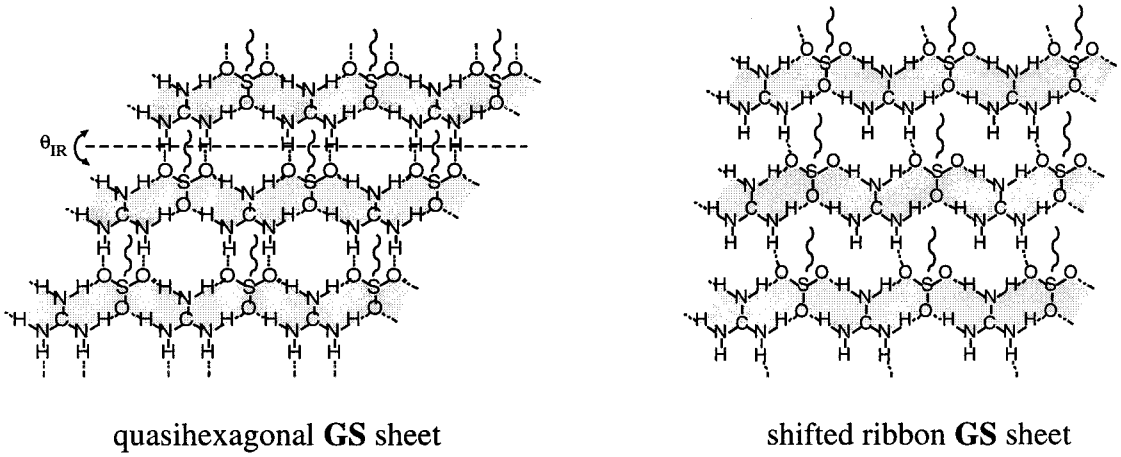

interdigitated layers in which the organic residues alternate to opposite sides of a given **GS** sheet. These properties illustrated the benefits of crystal engineering approaches based on *flexible* 2-D networks that can tolerate differently sized ancillary groups.

Our laboratory has exploited the unique properties of the **GS** network to synthesize a series of crystalline clathrates with host frameworks based on **G** ions and organo*di*sulfonates. These materials also exhibit lamellar ordering but with the organodisulfonate ions connecting opposing **GS** sheets to generate "pillared" galleries between the sheets.[9] The galleries contain (1-D) pores that can be occupied by a rather diverse variety of guest molecules. The size and shape of the pores can be tailored directly by judicious choice of the molecular pillar (e.g., 1,2-ethane-, 1,4-butane-, 2,6-naphthyl-, or 4,4′-biphenyldisulfonate). Notably, the 2-D **GS** network does not allow multifold interpenetration and the associated loss of framework porosity, a problem commonly encountered in crystalline clathrates and porous molecular frameworks.[10−14] The ability to retain the GS motif while modifying the host framework through introduction of different pillars provides a facile and versatile route to tunable inclusion environments.

The guanidinium organodisulfonate host can conceivably assemble into two different architectures that are best described as "bilayer" and continuous "brick" frameworks (Figure 1), the latter having nominally twice the pore volume as the bilayer form. Both isomers have been observed for host lattices based on the 4,4′-biphenyldisulfonate (**BPDS**) pillar. The bilayer architecture, having the formula $(\mathbf{G})_2(\mathbf{BPDS})\cdot$(guest), was observed for a rather diverse variety of aromatic guests.[15] However, 1,4-dibromobenzene (DBB), 1,4-divinylbenzene (DVB), 1-nitronaphthalene (NN), and nitrobenzene (NB) guests promoted the formation of the brick framework.[16] The preference for the more open brick framework by DBB, DVB, and NN was attributed primarily to the increased steric demands of these molecular guests compared to those of guests included in the bilayer framework. In the case of NB, the selectivity was attributed to the ability of the larger voids to accommodate

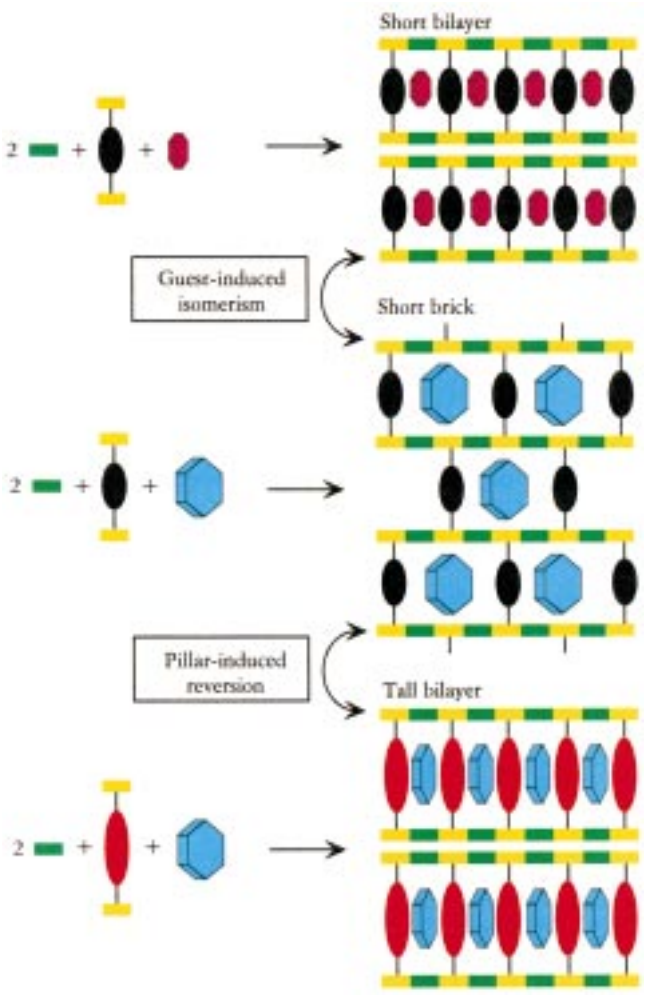

Figure 1. Schematic representations of a short bilayer (top), short brick (center), and tall bilayer (bottom) assembled from guanidinium ions (green), organodisulfonates (yellow for SO_3^- groups, black and red for short and tall organic residues, respectively), and guests (red or blue). Large guests that are incapable of fitting in the short bilayer can template the formation of the brick architecture, which nominally has twice the void space as the bilayer and can pucker to create pockets that can hold the larger guests. For clarity, this puckering is not illustrated. The tall pillar increases the pore size of the bilayer architecture so that the larger guests can be accommodated.

(9) (a) Russell, V. A.; Evans, C. C.; Li, W.; Ward, M. D. *Science* **1997**, *276*, 575−579. (b) Swift, J. A.; Russell, V. A.; Ward, M. D. *Adv. Mater.* **1997**, *9*, 1183−1186.
(10) Ermer, O. *J. Am. Chem. Soc.* **1988**, *110*, 3747−3754.
(11) Simard, M.; Su. D.; Wuest, J. D. *J. Am. Chem. Soc.* **1991**, *113*, 4696−4698.
(12) Copp, S. B.; Subramanian, S.; Zaworotko, M. J. *J. Am. Chem. Soc.* **1992**, *114*, 8719−8720.
(13) Reddy, D. S.; Craig, D. C.; Rae, A. D.; Desiraju, G. R. *J. Chem. Soc., Chem. Commun.* **1993**, 1737−1739.
(14) Batten, S. R.; Hoskins, B. F.; Robson, R. *J. Am. Chem. Soc.* **1995**, *117*, 5385−5386.
(15) Swift, J. A.; Reynolds, A. M.; Ward, M. D. *Chem. Mater.*, in press.
(16) Swift, J. A.; Pivovar, A. M.; Reynolds, A. M. *J. Am. Chem. Soc.* **1998**, *120*, 5887−5894.

Table 1. Crystallographic Data for $(G)_2(ABDS)\cdot$Guest Clathrates

guest	1,4-dibromobenzene	1,4-divinylbenzene	nitrobenzene[d]	1-nitronaphthalene[e]
empirical formula	$C_{20}H_{24}Br_2N_8O_6S_2$	$C_{24}H_{30}N_8O_6S_2$	$C_{20}H_{25}N_9O_7S_2$[f]	$C_{24}H_{27}N_9O_8S_2$[f]
formula weight (g/mol)	696.41	590.68		
crystal habit	plate	rod	plate	powder
dimensions (mm^3)	0.25 × 0.13 × 0.025	0.38 × 0.08 × 0.06	0.34 × 0.22 × 0.08	
space group	$P\bar{1}$	$P\bar{1}$	$P\bar{1}$	$P\bar{1}$
a (Å)	6.1845(1)	6.1603(1)	7.1781(3)	6.062
b (Å)	7.2317(2)	7.2903(2)	7.3188(4)	7.075
c (Å)	15.5039(2)	15.9207(1)	16.7531 (7)	15.629
α (deg)	94.232(1)	95.679(1)	89.185(2)	93.31
β (deg)	99.868(1)	95.058(1)	89.696(2)	91.79
γ (deg)	90.512(1)	96.741(1)	62.094(1)	86.48
volume ($Å^3$)	681.12(2)	702.97(2)	777.70(6)	667.64
Z	1	1	1	
calculated density (g/cm^3)	1.698	1.395		
F(000)	350	310	240	
absorption coeff. (mm^{-1})	3.180	0.243	0.204	
θ range for data collection (deg)	1.34−25.07	1.29−25.02	1.22−24.98	
reflections collected	4984	4409	2660	
independent reflections	2366	2429	2660	
reflections with $I > 2\sigma(I)$	1870	2115	1973	
GOF[a]	1.091	1.054	1.122	
R^b	0.0643	0.0400	0.0673	
$R_w{}^c$	0.1593	0.0989	0.2000	

[a] $\mathrm{GOF} = \frac{\sum[w(F_o^2 - F_c^2)^2]}{(n-p)^{1/2}}$. [b] $R = \frac{\sum||F_o| - |F_c||}{\sum|F_o|}$. [c] $R_w = \left[\frac{\sum(w(F_o^2 - F_c^2)^2)}{\sum(w(F_o^2)^2)}\right]^{1/2}$, $w = \frac{q}{\sigma^2(F_o^2) + (aP)^2 + bP}$.

[d] Single crystal X-ray diffraction data allowed refinement of only the host framework of **(G)$_2$(ABDS)·NB**. The **NB** guest molecules could not be refined satisfactorily. [e] The quality of **(G)$_2$(ABDS)·NN** crystals was poor, prohibiting single-crystal X-ray diffraction. The data provided were obtained by powder diffraction. [f] Empirical formula based on ^{1}H NMR data.

sterically demanding double-decker stacks of NB molecules. The brick framework displayed the adaptive nature that is a signature of these materials, with the GS sheet puckering so that the host lattice can conform to the contour of the guests and achieve efficient host−guest packing.

The observation of framework isomerism prompted us to examine whether increasing the pore size through the use of a slightly longer pillar would promote reversion to the bilayer framework by creating more pore volume for the aforementioned guest molecules. We report herein that the bilayer-to-brick change in architecture observed for (**G**)$_2$(**BPDS**) with **DBB**, **DVB**, **NN**, and **NB** can be *reversed* by employing azobenzene-4,4′-disulfonate (**ABDS**) as a pillar. The "taller" **ABDS** pillar expands the gallery height so that the bilayer framework can accommodate these guests, indicating that the selectivity toward these architectures depends on the *combined* steric requirements of the pillars and guests. This unprecedented ability to control solid-state structure in such a predictable manner is a direct consquence of crystal engineering through use of the robust 2-D **GS** network.

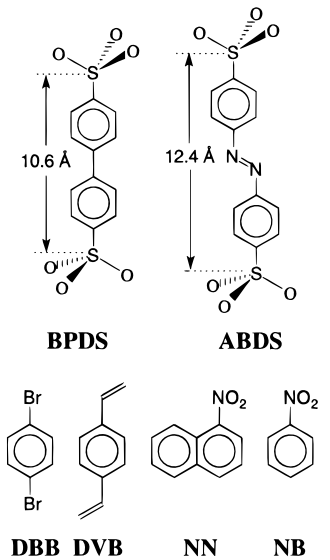

Results and Discussion

Salmon-colored plates of the (**G**)$_2$(**ABDS**)·(guest) clathrates were grown by slow evaporation of methanol solutions containing the appropriate guest and dissolved (**G**)$_2$(**ABDS**), which had been prepared in a prior step by metathesis of the acid form of **ABDS** and guandinium carbonate. Crystals suitable for single-crystal X-ray diffraction were obtained for (**G**)$_2$(**ABDS**)·**DBB**, (**G**)$_2$(**ABDS**)·**DVB**, and (**G**)$_2$(**ABDS**)·**NB**, whereas (**G**)$_2$(**ABDS**)·**NN** formed a microcrystalline powder that could only be analyzed by powder diffraction (Table 1). Unlike their **BPDS** analogues, all four clathrates form the bilayer architecture (Figure 1). Although single-crystal data was not available for (**G**)$_2$(**ABDS**)·**NN**, the existence of the bilayer architecture was verified from powder X-ray diffraction data.[17] Heating of the clathrates resulted in guest loss at temperatures exceeding 160 °C (see Experimental Section). Powder X-ray diffraction data of the guest-free (**G**)$_2$(**ABDS**) crystallized from methanol indicated poor crystallinity, suggesting that the bilayer framework could not be maintained in its original form in the absence of guests.

The single-crystal data reveal that the **ABDS** pillars connect opposing **GS** sheets, creating nonpolar galleries with one-dimensional pores flanked by the pillars. These pores are occupied by fully ordered rows of guest molecules that are commensurate with the host lattice (Figure 2 and 3). The **GS**

(17) The bilayer isomer can be distinguished from its brick counterpart by the relative intensities and positions of the d_{00l} reflections.

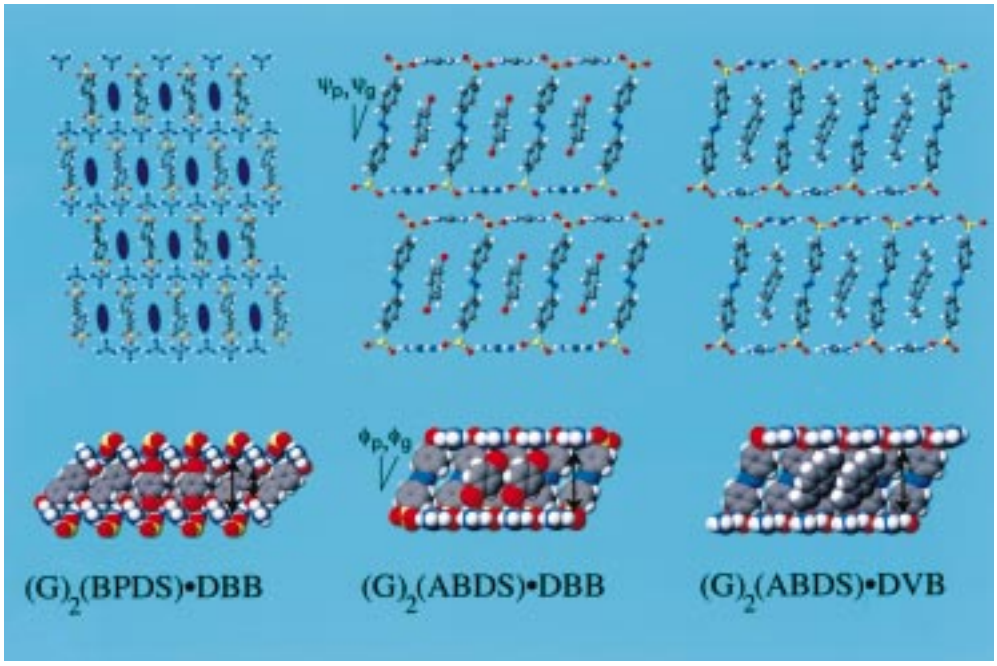

Figure 2. (**G**)$_2$(**BPDS**)·**DBB** brick (left), (**G**)$_2$(**ABDS**)·**DBB** bilayer (center), and (**G**)$_2$(**ABDS**)·**DVB** bilayer (right) frameworks as viewed along the one-dimensional channels in the galleries between the **GS** sheets (top) and normal to the channels (bottom). The representation of (**G**)$_2$(**BPDS**)·**DBB** is adapted from ref 5; the guests are depicted as ovals for clarity. The normal views depict the channel walls flanked by the **BPDS** or **ABDS** pillars. For clarity, only two guest molecules are depicted to illustrate the packing of the guests along the channel. Puckering of the brick (**G**)$_2$(**BPDS**) framework results in pockets with heights similar to the bilayer heights in the (**G**)$_2$(**ABDS**) framework. The 5.6 Å height of the pore aperture in (**G**)$_2$(**BPDS**)·**DBB**, as measured between guanidinium nitrogen atoms of opposing **GS** sheets, is depicted by the short arrrow. The 10.2 Å height of the puckered pocket, as measured between the closest sulfonate oxygen atoms of opposing **GS** sheets, is depicted by the long arrow. The bilayer pores of (**G**)$_2$(**ABDS**)·**DBB** and (**G**)$_2$(**ABDS**)·**DVB** have nominally uniform heights of 9.0 and 9.6 Å, respectively, as measured between the mean planes of guanidinium ions in opposing **GS** sheets. The angles used as a measure of pillar and guest-tilt are indicated. The structure of (**G**)$_2$(**BPDS**)·**DBB** is described in detail in ref 16.

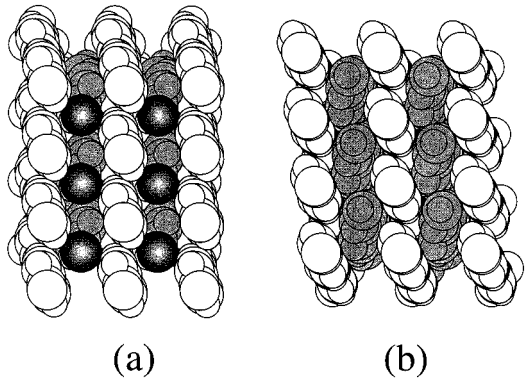

Figure 3. Space-filling representation of the gallery region of (a) (**G**)$_2$(**ABDS**)·**DBB** and (b) (**G**)$_2$(**ABDS**)·**DVB**, illustrating the herringbone packing of the aromatic rings of the guests and **BPDS** pillars. Guanidinium ions and sulfonate oxygen atoms in the top layer have been removed so that the packing of the guests and pillars can be observed. The Br atoms of the **DBB** guests are darkened for clarity.

sheets in (**G**)$_2$(**ABDS**)·**DBB** and (**G**)$_2$(**ABDS**)·**DVB** adopt the shifted-ribbon motif, as previously observed for the bilayer (**G**)$_2$(**BPDS**) clathrates.[9] The occurrence of the shifted-ribbon motif must reflect an optimized host−guest packing in the gallery region that outweighs the energetic penalty associated with loss of one hydrogen bond compared to the quasihexagonal motif. In contrast, (**G**)$_2$(**ABDS**)·**NB** displays the quasihexagonal motif.

Interestingly, the (**G**)$_2$(**ABDS**) host lattice exhibits a pronounced selectivity for 1,4-DVB. Crystallization from methanol solutions containing a commercial mixture of isomers (23%1,4-DVB, 57% 1,3-DVB, 17% 1,3-ethylvinylbenzene, and 17% 1,4-ethylvinylbenzene) produced crystalline (**G**)$_2$(**ABDS**) material with 86% 1,4-DVB included. Similar behavior was previously observed for the (**G**)$_2$(**BPDS**) brick clathrate.[16]

The pore structure in these materials also resembles that observed in the (**G**)$_2$(**BPDS**) bilayer clathrates. However, pore heights are necessarily greater in (**G**)$_2$(**ABDS**) bilayers than in (**G**)$_2$(**BPDS**) bilayers because of the 1.8 Å height difference between the two pillars (the height differences can be deduced from the projected intramolecular sulfur−sulfur distances of 10.6 and 11.4 Å for **BPDS** and **ABDS**, respectively). The phenyl rings in each **ABDS** pillar of (**G**)$_2$(**ABDS**)·**DBB**, (**G**)$_2$(**ABDS**)·**DVB**, and (**G**)$_2$(**ABDS**)·**NB** are coplanar. However, the azo moiety twists slightly out of the phenyl planes, the dihedral angles ranging from 1−6°. This degree of twist is comparable to that observed in solid *trans*-azobenzene.[18] The (**G**)$_2$(**ABDS**) host frameworks, neglecting guests, exhibit packing fractions near 0.5. If the guests are considered, the packing fractions exceed 0.7, typical of densely packed organic crystals. Determination of the **ABDS** geometry and packing fraction in (**G**)$_2$(**ABDS**)·**NN** was precluded by the absence of single-crystal diffraction data.

An obvious feature of the (**G**)$_2$(**ABDS**) clathrates is the absence of puckering, which is sterically prohibited for the bilayer architecture. Consequently, bilayer heights are fairly uniform among these clathrates, differing only slightly because of minor tilting of the pillars. Two angles, both subtending the long axis of the pillar and the normal to the **GS** sheet, are needed to completely describe the pillar tilt. One angle is measured when the structure is viewed perpendicular to the (1-D) pore (ϕ_p) and the other when viewed along the pore (ψ_p). The tilting of the pillars is accompanied by slight movement of the SO_3^-

(18) Brown, C. J. Acta Crystallogr. **1966**, *21*, 146−152.

Table 2. Structural Features of **(G)$_2$(ABDS)·Guest** Clathrates

guest	1,4-dibromobenzene	1,4-divinylbenzene	nitrobenzene
PF (without guest)[a]	0.54	0.52	0.47
PF (with guest)[a]	0.73	0.73	
ABDS tilt, view normal to pore (ϕ_p, deg)[b]	18	15	5
ABDS tilt, view parallel to pore (ψ_p,deg)[c]	15	12	1
guest tilt, view normal to pore (ϕ_g, deg)[b]	33	24	
guest tilt, view parallel to pore (ψ_g,deg)[c]	15	16	
ABDS dihedral twist angle (deg)[d]	6	1	3
pore direction	*a*	*a*	*a*
pore width (Å)[e]	7.2	7.3	7.3
estimated pore height[f]	9.0	9.6	10.7

[a] PF = packing fraction, calculated by Connolly surfaces using Cerius^2 molecular modeling software (version 1.6). A comparison of arbitrarily chosen examples from the Cambridge Structural Database revealed that the PF values calculated with Cerius^2 are systematically lower, by an average of 1.2%, than the Ck values reported by others [see Kitaigorodskii, A. I. *Molecular Crystals and Molecules*; Academic Press: New York, 1973 and Gavezzotti, A. *Nouv. J. Chim.* **1982**, *6*, 443]. [b] Tilt defined by the angle between the long axis of the **ABDS** or guest molecule and the normal to the **GS** mean plane, as viewed normal to the pore direction (see Figure 2). [c] Tilt defined by the angle between the long axis of the **ABDS** or guest molecule and the normal to the **GS** mean plane, as viewed parallel to pore direction (see Figure 2). [d] Dihedral angle between the azo moiety and the coplanar phenyl rings. [e] Pore widths are calculated from the center-to-center distance between **GS** ribbons, neglecting van der Waals radii. [f] Bilayer pore heights are calculated from the separation between the mean planes of opposing **G** ions, accounting for the van der Waals radii of the guanidinium carbon atoms.

Scheme 2

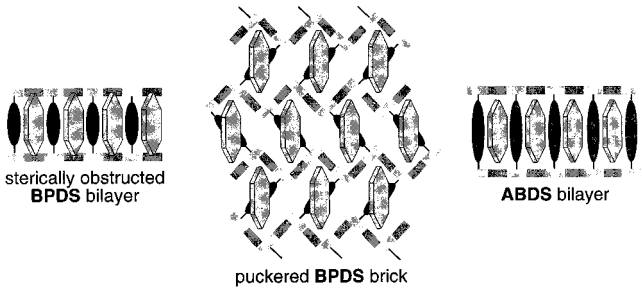

moieties out of the **GS** plane. Apparently, the energetic penalty resulting from less optimum hydrogen bonding is compensated by host−guest packing forces in the gallery region. The tilt of the guest molecules can be described by a convention similar to that of the pillars, using angles between the 1,4 axis of the guest and the normal to the GS sheet. As expected, in each case the guest-tilt when viewed along the pore (ψ_g) is essentially identical to ψ_p. However, the guest-tilt viewed perpendicular to the pore (ϕ_g) differs from ϕ_p. This can be attributed to the combination of achieving commensurism and optimizing guest−guest interactions in the pores.

The brick-to-bilayer reversion upon changing from **BPDS** to **ABDS** can be explained by a comparison of the pores in the (**G**)$_2$(**ABDS**) bilayer framework, the (**G**)$_2$(**BPDS**) brick framework, and an "ideal" (**G**)$_2$(**BPDS**) bilayer framework in which the pillars are oriented perpendicular to the **GS** sheet. Whereas the bilayer frameworks are not puckered, the **GS** sheets in the (**G**)$_2$(**BPDS**) brick frameworks are puckered to create corrugated, (1-D) pores. The pores are defined by small apertures separating larger "pockets" in which the molecule is included. The height of these pockets is larger than that which can be achieved in the ideal bilayer framework.[19] Thus, the puckering produces pore heights that can accommodate the protrusion of guest substituents that would be obstructed by the unpuckered **GS** sheets in the corresponding bilayer framework (Scheme 2). Although puckering results in energetically less favorable bent N−H···S hydrogen bonds, this is compensated by improved host−guest packing as the pockets conform to the contour of the guest molecules.

The actual pocket heights in the brick frameworks can be deduced from the distance between two sulfonate oxygen atoms on opposite sides of the pocket, based on the van der Waals radii of these atoms (r_{vdW} = 1.5 Å).[20] The bilayer pore heights can be calculated from the separation between the mean planes of opposing **GS** sheets, adjusted to account for the van der Waals radii of the guanidinium carbon atoms (r_{vdW} = 1.7 Å). These atoms were chosen in their respective frameworks because they represent the closest contacts between the guest molecules and the host.

The pocket heights calculated in this manner for the (**G**)$_2$(**BPDS**)·**DBB** and (**G**)$_2$(**BPDS**)·1.5 **DVB** brick clathrates are 10.2 and 11.0 Å, respectively. The smaller pocket height in the former is a consequence of the more severe tilting of the **BPDS** pillars and greater puckering ($\theta_{IR,DBB}$ = 63°; $\theta_{IR,DVB}$ = 130°). These characteristics can be attributed to the (**G**)$_2$(**BPDS**) host conforming to the shape of the smaller **DBB** guest in order to optimize host−guest interactions. In each case, the pocket heights exceed the maximum pore height of 7.8 Å that can be achieved by an ideal (**G**)$_2$(**BPDS**) bilayer framework.[19]

In contrast, the expansion of the bilayer in (**G**)$_2$(**ABDS**) that results from the longer **ABDS** pillar creates pore heights of 9.0 and 9.6 Å for (**G**)$_2$(**ABDS**)·**DBB** and (**G**)$_2$(**ABDS**)·**DVB**, respectively (Table 2).[21] In each case the pore height *exceeds* that of the ideal (**G**)$_2$(**BPDS**) bilayer, and the large guests can be accommodated in the bilayer (**G**)$_2$(**ABDS**) framework. In the case of (**G**)$_2$(**ABDS**)·**NB** the pore height of the bilayer framework is even larger (10.7 Å). The absence of a brick framework with double-decker stacks of **NB** guests, such as that observed for the **BPDS** analogue, suggests that this architecture would not result in efficient host−guest packing within the larger pores that would be created by the **ABDS** pillar. Although the **NB** guest moecules in (**G**)$_2$(**ABDS**)·**NB** could not be adequately refined, molecular models indicate that they can orient vertically in the bilayer pores. Such an orientation may facilitate weak hydrogen bonding between the nitro group of the guest and the guanidinium protons of the host, thereby stabilizing the bilayer framework and making a brick-like architecture with stacked guests less energetically preferable.

(19) The maximum pore height for the ideal (**G**)$_2$(**BPDS**) bilayer is defined by the distance between two opposing **GS** sheets in which the G ions and S oxygen atoms are coplanar, using the van der Waals radii of the guanidinium carbon atoms.

(20) Bondi, A. *J. Phys. Chem.* **1964**, *68*, 441−451.

(21) The 0.5 Å difference between the pore heights for the two bilayers reflects a small difference in minor tilting of the **ABDS** pillars that is accompanied by slight movement of the sulfonate moiety out of the mean **GS** plane. The tilt angles of the ABDS pillars, viewed normal to the pore direction and measured from the normal to the **GS** sheet, are 18 and 15 for (**G**)$_2$(**ABDS**)·**DBB** and (**G**)$_2$(**ABDS**)·**DVB**, respectively.

The formation of the bilayer framework also obviates the extensive puckering of the **GS** sheet that occurs in the brick architecture, thereby avoiding the formation of bent N−H···S hydrogen bonds.

Conclusion

Our previous observations of architectural isomerism, in which large guests incapable of fitting in the (**G**)$_2$(**BPDS**) bilayer framework templated the formation of a predictable brick framework with high porosity, established that the solid-state architecture of these clathrates could be rationally manipulated by judicious choice of the guest molecules. The results described here provide a second crucial element for crystal engineering of these systems. For a given guest, this change of architecture can be reversed by substituting longer molecular pillars that increase the pore size of the bilayer. This demonstrates that it is the *combined* steric requirements of the pillars and guests that govern which framework is adopted and argues that the host architecture of these materials can be rationally manipulated by systematic, stepwise changes in the size of the host and guest components. Additionally, these results illustrate that crystal engineering is simplified when structurally robust supramolecular elements are employed. In this case, the reliability of the **GS** sheets reduces design to the last remaining dimension so that structure prediction and control are feasible. The ability to tune the void volume of these frameworks to adjust to the steric demands of different guests while retaining the lamellar ordering provides extraordinary versatility that can substantially advance the design and synthesis of novel functional materials.

Experimental Section

Materials and Methods. Reagents purchased from commercial sources were used as obtained without further purfication. The compositions of the clathrates were verified by ^{1}H NMR, using samples dissolved in DMSO-d_6. The temperatures at which appreciable amounts of guest were first lost from the clathrates and melting points were determined by differential scanning calorimetry (Perkin-Elmer Pyris 1).

X-ray Diffraction. Powder diffraction data were collected with a Siemens D-500 or D-5005 diffractometer with a Cu source ($\lambda = 1.542$ Å). Single crystals at 173(2) K were examined via hemisphere collection on a Siemens SMART Platform CCD diffractometer. A graphite monochromator was used with Mo Kα radiation ($\lambda = 0.71073$ Å). Direct methods (SHELXTL-V5.0, Siemens Industrial Automation, Inc.) were employed to solve the structures, which were refined using full-matrix least-squares/difference Fourier techniques. All non-hydrogen atoms were refined with anisotropic displacement parameters, while all hydrogen atoms were placed in idealized positions and refined as riding atoms with the relative isotropic displacement parameters. The Siemens Area Detector ABSorption program (SADABS) was used for absorption corrections.[22]

Synthesis of Guanidinium Azobenzene-4,4′-disulfonate. The sodium salt of azobenzene-4,4′-disulfonic acid was prepared from sulfanilic acid (Aldrich, 99%) by diazonium coupling.[23] The sodium salt (12.04 g, 31.18 mmol) was dissolved in deionized water and converted to the barium salt by adding an aqueous solution of $BaCl_2$ (10% excess). The BaABDS precipitate was isolated by centrifugation, dried, and mixed with 10% excess of H_2SO_4 in 10 mL of H_2O. The resulting slurry was centrifuged to remove $BaSO_4$, and the supernatant liquid was added to an aqueous solution containing a stoichiometric amount of guanidinium carbonate (Aldrich, 99%). The solvent was removed in vacuo to afford 11.82 g of crude (**G**)$_2$(**ABDS**), which was recrystallized four times from methanol (overall yield after recrystallization, based on the sodium salt: 7.01 g, 48.8%). ^{1}H NMR δ 7.93 (dd, 4H, $J = 1.8$, 6.6 Hz), 7.81 (dd, 4H, $J = 1.8$, 6.8 Hz), 6.94 (s, 12H). Elemental analysis (MHW Laboratories, Phoenix, AZ) Calcd for $C_{14}H_{20}N_8O_6S_2$: C, 36.51; H, 4.38; N, 24.33; S, 13.92%. Found: C, 34.67; H, 4.56; N, 23.51; S, 13.24%. mp = 248−250 °C.

Crystal Growth of (G)$_2$(ABDS)·DBB. Equimolar amounts of (**G**)$_2$(**ABDS**) (100 mg, 0.22 mmol) and 1,4-dibromobenzene (51.2 mg, 0.22 mmol) were dissolved in 10 mL of boiling methanol. The solution was allowed to cool, resulting in the formation of salmon-colored crystals that were retrieved by filtration. The stoichiometry of the clathrate was confirmed by ^{1}H NMR (Varian 300 MHz, DMSO-d_6) δ 7.89 (dd, 4H, $J = 1.2$, 8.7 Hz), 7.81 (dd, 4H, $J = 0.9$, 8.1 Hz), 7.55 (m, 4H), 6.94 (s, 12H). Guest loss was first observed at 231 °C; mp = 263−286 °C.

Crystal Growth of (G)$_2$(ABDS)·DVB. (**G**)$_2$(**ABDS**) (100 mg, 0.22 mmol) and 1,4-divinylbenzene (1 mL, 0.91 mmol; Aldrich, 80%, mixture of isomers) were dissolved in 10 mL of boiling methanol. The solution was allowed to cool, resulting in the formation of salmon-colored crystals that were retrieved by filtration. Gas chromatography revealed that the starting material consisted of 23% 1,4-divinylbenzene, 57% 1,3-divinylbenzene, 17% 1,3-ethylvinylbenzene, and 17% 1,4-ethylvinylbenzene. Analysis of the guest included in (**G**)$_2$(**ABDS**) afforded concentrations of 86, 8, 0, and 6%, respectively, for these materials, indicating significant selectivity for 1,4-DVB. Consequently, the crystal structure was refined assuming a 100% occupancy of the 1,4 isomer of DVB. The ^{1}H NMR spectrum of solutions prepared by dissolving harvested crystals confirmed that 1,4-DVB was the predominant guest with trace amounts of 1,3-DVB and 1,4-ethylvinylbenzene: δ 7.89 (dd, 4H, $J = 2.1$, 6.6 Hz), 7.82 (dd, 4H, $J = 2.1$, 6.9 Hz), 7.46 (s, 4H), 6.94 (s, 12H), 6.74 (m, 2H), 5.85 (dd, 2H, $J = 0.9$, 17.7 Hz), 5.27 (dd, 2H, $J = 1.6$, 9.4 Hz). Guest loss was first observed at 160 °C; mp = 224−230 °C.

Crystal Growth of (G)$_2$(ABDS)·NB. (**G**)$_2$(**ABDS**) (100 mg, 0.22 mmol) and nitrobenzene (1 mL, 1.2 mmol; Aldrich, 99%) were dissolved in 10 mL of boiling methanol. The solution was allowed to cool, resulting in the formation of salmon-colored crystals that were retrieved by filtration. The stoichiometry of the clathrate was confirmed by ^{1}H NMR δ 8.25 (m, 2H), 8.075 (dd, 1H, $J = 1.5$, 8.4 Hz), 7.90 (m, 4H), 7.82 (m, 4H), 7.72 (m, 2H), 6.95 (s, 12H). Guest loss was first observed at 198 °C; mp = 242−277 °C. The single-crystal X-ray diffraction data for (**G**)$_2$(**ABDS**)·**NB** were not adequate for refinement of the guest molecules, owing to poor crystal quality. The **NB** guest molecules were disordered, presumably as a consequence of partial loss of the guests from the host. PLATON/SQUEEZE [24] was used to remove the effects of this disorder from the data so that the structure of the host could be refined satisfactorily. Some atoms exhibit large anisotropic displacement parameters.

Crystal Growth of (G)$_2$(ABDS)·NN. Equimolar amounts of (**G**)$_2$(**ABDS**) (100 mg, 0.22 mmol) and 1-nitronaphthalene (38 mg, 0.22 mmol; Aldrich, 99%) were dissolved in 10 mL of boiling methanol. The solution was allowed to cool, resulting in the formation of a microcrystalline powder that was retrieved by filtration. The stoichiometry of the clathrate was confirmed by ^{1}H NMR: δ 8.36 (m, 3 H), 8.19 (dd, 1H, $J = 0.9$, 8.4 Hz), 7.89 (dd, 4H, $J = 1.5$, 8.1 Hz), 7.80 (m, 7H), 6.94 (s, 12H). Guest loss occurred above 200 °C, mp = 222−233 °C.

Acknowledgment. We are grateful to Victor G. Young, Jr., of the X-ray Crystallographic Laboratory of the University of Minnesota for X-ray diffraction analysis and to Dr. J. A. Swift and Mr. A. Pivovar for furnishing the structural details of the brick clathrates. We also acknowledge financial support from the National Science Foundation and the Center for Interfacial Engineering, an NSF Engineering Research Center at the University of Minnesota.

Supporting Information Available: Tables of X-ray data, collection and refinement parameters, atomic position parameters, anisotropic displacement parameters, and thermal ellipsoid plots for (**G**)$_2$(**APDS**)·**DBB**, (**G**)$_2$(**APDS**)·**DVB**, and (**G**)$_2$(**APDS**)·**NB** (32 pages, PDF). See any current masthead page for Web access instructions.

JA983122O

(22) Blessing, R. *Acta Crystallogr.* **1995**, *A51*, 33−38.
(23) Clarke, H. T. *J. Org. Chem.* **1971**, *36*, 3816−3819.
(24) Spek, A. L. *Acta Crystallogr.* **1990**, *A46*, C34.